CORE
Metadata, citation and similar papers at core.ac.uk
Provided by CURVE/open

Scaling behavior of the Heisenberg model in three dimensions

Gordillo-Guerrero, A. , Kenna, R. and Ruiz-Lorenzo, J.J.

Published version deposited in CURVE April 2014

Original citation & hyperlink:
Gordillo-Guerrero, A. , Kenna, R. and Ruiz-Lorenzo, J.J. (2013) Scaling behavior of the Heisenberg model in three dimensions. Physical Review E - Statistical, Nonlinear, and Soft Matter Physics, volume 88 (6): 062117.
http://dx.doi.org/10.1103/PhysRevE.88.062117

Publisher statement: © 2013 American Physical Society.

Copyright © and Moral Rights are retained by the author(s) and/ or other copyright owners. A copy can be downloaded for personal non-commercial research or study, without prior permission or charge. This item cannot be reproduced or quoted extensively from without first obtaining permission in writing from the copyright holder(s). The content must not be changed in any way or sold commercially in any format or medium without the formal permission of the copyright holders.

CURVE is the Institutional Repository for Coventry University
http://curve.coventry.ac.uk/open

Scaling behavior of the Heisenberg model in three dimensions

A. Gordillo-Guerrero,[1,2] R. Kenna,[3] and J. J. Ruiz-Lorenzo[2,4]

[1]*Departamento de Ingeniería Eléctrica, Electrónica y Automática, Universidad de Extremadura, Avda Universidad s/n, Cáceres, 10071, Spain*

[2]*Instituto de Biocomputación and Física de Sistemas Complejos (BIFI), Zaragoza, 50009, Spain*

[3]*Applied Mathematics Research Centre, Coventry University, Coventry, CV1 5FB, England*

[4]*Departamento de Física, Universidad de Extremadura, Avda Elvas s/n, Badajoz, 06071, Spain*

(Received 23 July 2013; published 10 December 2013)

We report on extensive numerical simulations of the three-dimensional Heisenberg model and its analysis through finite-size scaling of Lee-Yang zeros. Besides the critical regime, we also investigate scaling in the ferromagnetic phase. We show that, in this case of broken symmetry, the corrections to scaling contain information on the Goldstone modes. We present a comprehensive Lee-Yang analysis, including the density of zeros, and confirm recent numerical estimates for critical exponents.

DOI: 10.1103/PhysRevE.88.062117 PACS number(s): 64.60.−i

I. INTRODUCTION

The universality concept is commonly stated together with the hypotheses of scaling and finite-size scaling for thermodynamic functions close to the critical points associated with continuous phase transitions. The theory of finite-size scaling has been very successful in predicting critical and noncritical properties of bulk systems from those of their finite or partially finite counterparts [1]. Although comparisons between experiment and theory, as well as between the variety of theoretical approaches, yield good overall agreement in the main, difficulties in reconciling details of scaling in a number of important experiments remain [2,3]. These include some experimental realizations of systems with continuous symmetry groups, such as the those in the three-dimensional O(3) Heisenberg universality class, including isotropic ferromagnets with and without quenched disorder, e.g., Ni, EuO, and $La_{1-x}A_xMnO_3$. Precise theoretical estimates for the critical temperature and critical exponents are contained in Refs. [4–6] for the pure and site-diluted Heisenberg models with quenched disorder. A review of theoretical and experimental measurements of critical exponents for the Heisenberg model is contained in Ref. [7].

Here we present results from a theoretical study of the Heisenberg model in three dimensions. Our objective is not to revisit old ground but to investigate the Lee-Yang (LY) zeros [8] of this continuous-symmetry-group model through Monte Carlo simulations. We do this through finite-size scaling, primarily at the critical point, but also in the ferromagnetic regime.

A first motivation is to investigate the Goldstone modes in the broken phase, which affect the corrections to scaling there. Although there are many studies in the literature of how Goldstone modes are manifest in terms of the physics of such systems (e.g., see Ref. [9]), their effects on complex singularities have not previously been investigated. In particular, Refs. [10,11] contained finite-size investigations of the critical behavior of vector models, taking into account the Goldstone modes,[1] theoretical results that subsequently were tested numerically in Ref. [12]. More recently, for instance, Dohm studied the influence of Goldstone modes on the Casimir effect [13].

Physical interpretations for complex singularities are established in Ref. [14]. In particular, the Yang-Lee edge is a manifestation of the symmetric phase, and this has not previously been analyzed numerically in the Heisenberg model. We also investigate the crossover in the detailed behavior of zeros from the ferromagnetic to critical phases. We show that a simple scaling prescription in terms of the index of zeros ceases to be valid as criticality is approached. The change in behavior of the density of zeros between the phases is also investigated. Another motivation, therefore, is to compute critical exponents using a technique not used so far in this model in order to provide numerical data from an independent angle.

Finally, full understanding of the scaling behavior (including the associated correction-to-scaling) of the LY zeros in the ferromagnetic region for Heisenberg models is further motivated by its relevance for the understanding of the Griffiths phase in disordered models with continuous symmetry, which have been of increased interest in recent years, mainly in experimental studies.[2] Colossal magnetoresistance is an example of a Griffiths singularity for Heisenberg materials [17].

In the next section we outline the Heisenberg model and briefly discuss the observables we focus on in this paper. In Sec. III we give details of the Monte Carlo simulations.

[1]Note that Ref. [11] works in the limit $hV =$ constant, where h is the magnetic field and V the volume of the system. Here, we have performed all the numerical simulations at $h = 0$, so this limit is not directly applicable to our work.

[2]In diluted ferromagnets, for example, the region above the critical temperature of the disordered model and below the critical temperature of the pure model is called the Griffiths phase. In this phase the free energy is not analytic as it is in a typical paramagnetic phase. The nonanalyticity of the free energy does not induce a phase transition in the static but changes the functional form of the equilibrium correlation function [15]. Griffiths showed how this phase can be interpreted in terms of the LY zeros [16]. In the Griffiths phase, the LY zeros associated with large and ordered spin domains reach the real axis, but with a density of the zeros insufficient to induce a true phase transition in the static of the model.

 ©2013 American Physical Society

The outcomes of the simulations are analyzed in Sec. IV. A compact scaling description in terms of densities of zeros is given in Sec. V, and we conclude in Sec. VI. Finally, in the Appendix we describe the limitations of our numerical method for characterizing the Yang-Lee edge (YL edge) in the paramagnetic phase.

II. MODEL AND OBSERVABLES

The Heisenberg model in d dimensions may be defined in terms of O(3) spin variables placed at the nodes of a cubic lattice. The volume of the lattice is $V = L^d$, where L is its linear size and the lattice constant has been set to one. The model is governed by a Hamiltonian $\mathcal{H}$ given by

$$\beta\mathcal{H} = -\beta \sum_{\langle i,j \rangle} \boldsymbol{S_i} \cdot \boldsymbol{S_j} - \boldsymbol{h} \cdot \sum_i \boldsymbol{S_i}. \tag{2.1}$$

Here $\beta = 1/(k_B T)$, where T is the temperature and $\boldsymbol{h}$ is an external magnetic field. The $\boldsymbol{S_i}$ are three-dimensional vectors of unit modulus, and the first sum is extended only over nearest neighbors. We henceforth set the Boltzmann constant k_B to unity. We define the total nearest-neighbor energy as

$$E = -\sum_{\langle i,j \rangle} \boldsymbol{S_i} \cdot \boldsymbol{S_j} \tag{2.2}$$

and the total magnetization density as a three-component vector

$$\boldsymbol{M} = (M_x, M_y, M_z) = \sum_i \boldsymbol{S_i}. \tag{2.3}$$

The partition function is

$$Z_L(T,h) = \sum_{\{S_i\}} \exp\left(-\beta\mathcal{H}\right) = \sum_{\{S_i\}} \exp\left(-\beta E + \boldsymbol{h} \cdot \boldsymbol{M}\right). \tag{2.4}$$

The susceptibility is defined through the derivatives

$$\nabla_h \ln Z = \frac{1}{V} \langle \boldsymbol{M} \rangle, \tag{2.5}$$

$$\chi_L(T,h) = \frac{1}{V} {\nabla_h}^2 \ln Z_L(T,h) = \frac{1}{V}(\langle \boldsymbol{M}^2 \rangle - \langle \boldsymbol{M} \rangle^2), \tag{2.6}$$

in which the thermal average is denoted by $\langle \cdots \rangle$. Because the probability of reaching every minimal value for the free energy is nonvanishing, the thermal average of Eq. (2.3) is zero in the absence of an external field, for a finite lattice. While this is an accurate finite-size counterpart for the susceptibility in the symmetric phase, it cannot be used to capture the connected susceptibility in the broken phase. Therefore we have to introduce separate definitions for the connected and nonconnected finite-size susceptibilities, namely,

$$\tilde{\chi}_L(T, h = 0) = \frac{1}{V}(\langle \boldsymbol{M}^2 \rangle - \langle |\boldsymbol{M}| \rangle^2) \tag{2.7}$$

and

$$\chi_L^{(\mathrm{nc})}(T, h = 0) = \frac{1}{V}\langle \boldsymbol{M}^2 \rangle. \tag{2.8}$$

For numerical measurements on a finite lattice it is appropriate to use $\tilde{\chi}_L$ and $\chi_L^{(\mathrm{nc})}$ in the ferromagnetic and paramagnetic regimes, respectively. One should not use $\tilde{\chi}_L$ in the paramagnetic phase because, unlike $\langle \boldsymbol{M} \rangle$, $\langle |\boldsymbol{M}| \rangle$ does not vanish there for finite-size systems. Indeed, the usage of $\langle |\boldsymbol{M}| \rangle$ in the symmetric phase would be tantamount to the introduction of a nonvanishing external field there. There is no order parameter for finite-size systems (because they do not manifest a phase transition), but $\chi_L^{(\mathrm{nc})}$ and $\tilde{\chi}_L$ each approach χ_∞ in the thermodynamic limit.

Inspired by the fundamental theorem of algebra, Lee and Yang introduced the idea of complex zeros of the partition function as a way to investigate the onset and properties of phase transitions [8]. The resulting approach constitutes a fundamental theory of phase transitions [18]. In the paramagnetic phase, the LY zeros in the complex h plane remain away from the real magnetic-field axis, as proved in Ref. [19]. This means there exists a gap on the imaginary h axis in which the density of zeros is zero. The free energy is analytic in h in the gap and no phase transition can occur as a function of h. The ends of the nonvanishing distribution of zeros was termed the Yang-Lee edge in Ref. [20]. The proof that the LY zeros of the partition function are located on the imaginary h axis for the Heisenberg ferromagnet was given in Ref. [21]. Here we present a numerical investigation into the LY zeros for the model in three dimensions.

Following Ref. [22], for example, in order to find the LY zeros of the system we write the partition function in an imaginary field of strength ir as

$$Z_L(T, ir) = Z_L(T,0)\langle \cos(rM) + i \sin(rM) \rangle, \tag{2.9}$$

where M is the component of $\boldsymbol{M}$ picked out by the field. Here the thermal average is a real measure, taken with $Z(T,h = 0)$. Since the mean value of an observable which is not invariant under O(3) is automatically zero, odd moments of the magnetization vanish. Therefore the partition function in a pure imaginary magnetic field is real and the zeros are given by $\langle \cos(rM) \rangle = 0$. In the ferromagnetic phase, and in analogy with Eq. (2.7), one may use for M the modulus $|\boldsymbol{M}|$. Then one seeks the zeros as solutions to

$$\langle \cos(r|\boldsymbol{M}|) \rangle = 0. \tag{2.10}$$

However, just as Eq. (2.7) is inappropriate in the high-temperature phase, so is Eq. (2.10) unsuitable there. Instead, and in analogy to Eq. (2.8), one has to use an explicit component for M, say $M = M_x$:

$$\langle \cos(rM_x) \rangle = 0. \tag{2.11}$$

In this way we can attempt to obtain the zeros of the partition function for each L in the various regimes. The resulting jth, temperature-dependent, LY zero is denoted by $r_j(T; L)$, the zero with $j = 1$ being the smallest.

A. Scaling of the thermodynamic functions and zeros

In the limit of infinite volume, the standard expressions for the leading thermal scaling are $\chi_\infty(T) \sim |t|^{-\gamma}$, $m_\infty(h) \sim h^{1/\delta}$, $\xi_\infty(T) \sim |t|^{-\nu}$, and $r_1(T) \sim t^\Delta$, for $t > 0$. Here, t is the reduced temperature, $(T - T_c)/T_c$, and we suppress writing explicit dependency on h or t when they vanish. In the following, we focus on the finite-size scaling (FSS) of the susceptibility and zeros. According to standard FSS theory, these are obtained through the substitution $\xi_\infty(T) \to \xi_L(T_c) \sim L$ or $t \to L^{-1/\nu}$. Therefore we expect to extract the leading

scaling behavior through

$$\chi_L(T_c) \sim L^{\frac{\gamma}{\nu}}, \quad r_j(T_c;L) \sim L^{-\frac{\Delta}{\nu}}. \tag{2.12}$$

We can estimate γ/ν and Δ/ν through the scaling relations

$$\frac{\gamma}{\nu} = 2-\eta \quad \text{and} \quad \frac{\Delta}{\nu} = \frac{d+2-\eta}{2}, \tag{2.13}$$

provided the anomalous dimension η is known. The most recent measurement of this critical exponent is $\eta = 0.0378(3)$ [6], and from this one obtains

$$\frac{\gamma}{\nu} = 1.9622(3) \quad \text{and} \quad \frac{\Delta}{\nu} = 2.4811(2). \tag{2.14}$$

These values are used throughout this work.

B. Compact scaling of Lee-Yang zeros

In Ref. [23], it was suggested that the partition function zeros could scale, in the critical region, as a fraction of the total number of zeros, i.e., as a function of j/L^d, for large values of the index j. In fact, many models give scaling in the ratio $(j-\epsilon)/L^d$ in which $\epsilon = 1/2$ [24,25]. If such a functional form is widespread for LY zeros, it suggests that Eq. (2.12) be promoted to the more comprehensive form

$$r_j(T;L) \sim \left(\frac{j-\epsilon}{L^d}\right)^{C(T)} \tag{2.15}$$

for $T \leqslant T_c$. To investigate this further, first write the finite-size partition function in terms of its LY zeros as

$$Z_L(T,h) = A\prod_{j=1}^{V/2}(h-h_j)(h-h_j^*), \tag{2.16}$$

where A is nonvanishing (as a function of h) and $*$ means complex conjugation. Then the susceptibility is

$$\chi_L(T) = -\frac{1}{V}\sum_{j=1}^{V/2}\left(\frac{1}{h_j^2}+\frac{1}{h_j^{*2}}\right). \tag{2.17}$$

When the Lee-Yang theorem [8] holds and $h_j = ir_j$ is purely imaginary, this gives that

$$\chi_L(T) = \frac{2}{V}\sum_{j=1}^{V/2}\frac{1}{r_j^2(T;L)}. \tag{2.18}$$

Equation (2.18) relates the LY zeros to the susceptibility defined through Eq. (2.6), i.e., through the second derivative of the partition function. To gain insight into the behavior of the zeros away from criticality, we consider the $T \to 0$ and $T \to \infty$ limits of this susceptibility. For a finite-size system, the full susceptibility χ_L from Eq. (2.6) coincides with the nonconnected version $\chi_L^{(\mathrm{nc})}$ defined through Eq. (2.8), and at low temperatures, $\chi_L(T \ll 1) = \chi_L^{(\mathrm{nc})}(T \ll 1) \simeq V$. If $T \to \infty$, on the other hand, $\chi_L(T \to \infty) = \chi_L^{(\mathrm{nc})}(T \to \infty) = 1$. Note that these are different from the modified susceptibility $\tilde{\chi}_L(T)$ as defined in Eq. (2.7). This is only used as a replacement for $\chi_L(T)$ below T_c and, in the low-temperature limit where the spins align, it is $\tilde{\chi}_L(T=0) = 0$. However, even in the paramagnetic phase, it is the susceptibility χ_L (equivalently $\chi_L^{(\mathrm{nc})}$) and not $\tilde{\chi}_L$ that is related to the LY zeros through Eq. (2.18).

In the absence of a YL edge, when the zeros can pinch the real axis, we assume the form (2.15) for the comprehensive scaling of the zeros. Inserting into Eq. (2.18), one finds that the leading finite-size behavior of the susceptibility is

$$\chi_L(T) \sim L^{d(2C-1)}, \tag{2.19}$$

which comes from the contributions from the lowest zeros.

This recovers the FSS formula (2.12) in the critical regime provided $C(T_c) = \Delta/\nu d$. It also recovers the scaling $\chi_L(T < T_c) \sim L^d$ in the ferromagnetic phase if $C = 1$ there. The ansatz (2.15) fails in the paramagnetic phase, however, because, it does not take into account the Yang-Lee edge and, plugged into Eq. (2.18), it would lead to a spurious logarithmic divergence in the susceptibility there.

C. Corrections to scaling

At the critical point, the corrections to leading finite-size scaling are governed by the ω exponent. For the susceptibility and LY zeros, one expects

$$\chi_L(T_c) \sim L^{\frac{\gamma}{\nu}}[1+\mathcal{O}(L^{-\omega})], \tag{2.20}$$

$$r_j(T_c;L) \sim L^{-\frac{\Delta}{\nu}}[1+\mathcal{O}(L^{-\omega})]. \tag{2.21}$$

The widely accepted measured value for the correction exponent is $\omega \approx 0.8$ [5,7].

Away from the critical temperature one may also expect corrections to scaling. Since the model under consideration has a continuous symmetry group, the effects of Goldstone modes in the ferromagnetic regime are of interest (the ferromagnetic phase is also critical). Since these modes are massless, the corresponding propagator is $1/p^2$ in momentum space, producing an L^2 divergence in the connected susceptibility. The longitudinal susceptibility, on the other hand, diverges as $1/p^{4-d} = 1/p$, inducing a correction proportional to L. Therefore the susceptibility for the Heisenberg model in the ferromagnetic phase (in the presence of Goldstone modes) may be expected to scale as (see also Refs. [11,12])

$$\chi_L(T < T_c) \sim L^3[1+\mathcal{O}(L^{-1})+\mathcal{O}(L^{-2})]. \tag{2.22}$$

In the Ising case, on the other hand, the absence of Goldstone modes suggests the absence of such correction. There, one expects Eq. (2.22) to be replaced by $\chi_L(T < T_c) \sim L^3[1+\mathcal{O}(L^{-3})+\mathcal{O}(L^{-3}\exp(-L/\xi))]$, where we have added the (next-to-leading) finite-size correction (the exponential term), where ξ is the correlation length. Notice that the leading corrections are given by the bulk behavior of the connected susceptibility (divergent in vector models due to the transverse and longitudinal modes) and constant (proportional to $1/\xi^2$) in the Ising case.

Therefore the corrections to scaling in the broken phase deliver information on the existence of Goldstone modes. As we have seen, the LY zeros are closely related to the susceptibility. They may therefore be expected to carry the same correction-to-scaling behavior. One then expects, for the zeros in the low-temperature phase,

$$r_j(T < T_c;L) \sim L^{-d}[1+\mathcal{O}(L^{-1})]. \tag{2.23}$$

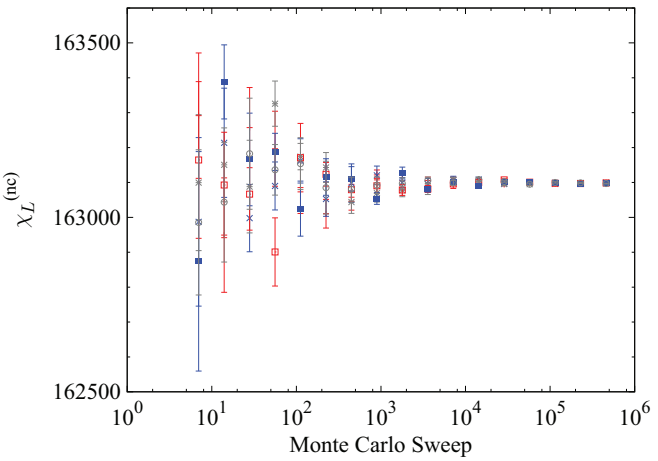

FIG. 1. (Color online) Log-binning of susceptibility for five random chosen independent Monte Carlo runs with $L = 64$ simulated at $T = T_c/2$. Error bars are typical deviations in each bin. The first bin only includes seven measurements, explaining the deviations for small times.

Combining with the index dependency suggested in the previous subsection, one expects a comprehensive scaling behavior for the LY zeros for the Heisenberg model as

$$r_j(T;L) = \left(\frac{j-\epsilon}{L^d}\right)^C [1 + \mathcal{O}(L^{-E})], \qquad (2.24)$$

with $C = \Delta/\nu d$ and $E = \omega$ when $T \approx T_c$, and $C = 1$ and $E = 1$ when $T \ll T_c$.

III. SIMULATION DETAILS

We simulated the Heisenberg model on regular, cubic lattices with linear sizes $L = 8$, 12, 16, 24, 32, 48, and 64. We used periodic boundary conditions, and in each case 20 independent Monte Carlo runs (pseudosamples) were used to average out the thermal noise. We performed our simulations at several different values of the system temperature. We use the estimate for the critical temperature $\beta_c = 1/T_c = 0.693$ from Ref. [26]. Apart from this value, we also simulated at two lower temperatures, $T = 2T_c/3$ ($\beta = 1.039\,5$) and $T = T_c/2$ ($\beta = 1.386$), both in the ferromagnetic regime.

TABLE I. The Monte Carlo sweep size for each system size L. Here, N_{Wolff} denotes the number of Wolff updates performed after the partial Metropolis update.

L	8	12	16	24	32	48	64
N_{Wolff}	10	20	25	40	50	75	100

The update scheme involved the Metropolis method applied to over 10% of the individual spins, chosen at random, followed by a number (increasing with L) of cluster updates using a Wolff cluster method. See Table I for details. We refer to each one of these combined updates as a Monte Carlo sweep. After every Monte Carlo sweep we measure magnetization and energy, performing 10^6 measurements for every pseudosample.

In order to work with thermally equilibrated systems, we performed 10^5 Monte Carlo sweeps before starting measurements. We start the simulations from hot (random) distributions of the spin variables, although we have checked that the averages do not change if we begin with cold configurations (i.e., all spins pointing in the same direction). In Fig. 1, we compare the thermalization of the different pseudosamples in the most challenging case, i.e., our largest system at the lowest temperature. We performed a similar check for the log-binning of the specific heat.

IV. FINITE-SIZE SCALING

We begin our analysis with a brief discussion of FSS of the susceptibility in the critical and ferromagnetic regimes. As mentioned in the Introduction, our aim is not to generate new estimates for the critical temperature and critical exponents. Rather, we wish to examine some of the under-researched aspects of the Heisenberg model outlined in Sec. I. Therefore, we first check the consistency of our results with earlier studies before moving on to the LY zeros, which form the focus for our work. In Fig. 2 (left panel), the critical susceptibility data are plotted with a best fit to Eq. (2.20). We obtain acceptable fits using the data for $L > 16$. If we include the next scaling correction term, $\mathcal{O}(L^{-2\omega})$, we obtain a good fit using all the system sizes. The estimates $\gamma/\nu = 1.962\,2(3)$ and $\omega = 0.79$ from Ref. [6] are used. The fit confirms these estimates for the data. The susceptibility is also plotted in the ferromagnetic phase in Fig. 2 (right panel). The scaling

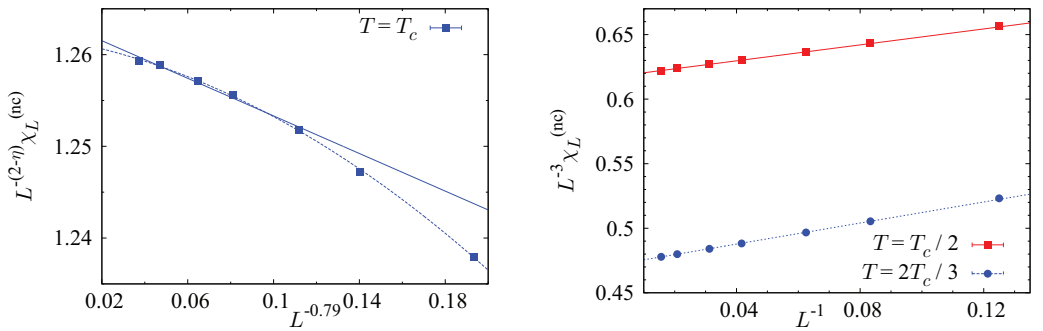

FIG. 2. (Color online) Finite-size scaling of the susceptibility at the critical point (left) and in the ferromagnetic regime (right), supporting the forms (2.20) and (2.22), respectively. In the left panel the dotted line includes next-to-leading corrections of the form $L^{-2\omega}$ in the fit. The error bars are smaller than the size of the symbols in each case.

TABLE II. The first four LY zeros for different lattice sizes at $T = T_c$.

L	$r_1(L)$	$r_2(L)$	$r_3(L)$	$r_4(L)$
8	0.00825415(59)	0.0243727(17)	0.0396287(27)	0.0541716(40)
12	0.00300815(27)	0.00888260(73)	0.0144417(12)	0.0197404(21)
16	0.00147165(14)	0.00434424(34)	0.00706250(50)	0.0096533(9)
24	0.000537193(39)	0.00158625(11)	0.00257895(18)	0.0035250(3)
32	0.000262952(19)	0.000776455(47)	0.001262269(74)	0.00172516(17)
48	0.000096098(9)	0.000283759(24)	0.000461266(37)	0.00063038(6)
64	0.000047062(4)	0.000138962(10)	0.000225888(16)	0.00030869(3)

form (2.22) is confirmed, including the corrections coming from the Goldstone modes.

To achieve relatively small error bars in estimating the zeros, we follow an iterative approach whereby we first estimate the location of the zeros by detecting changes in the sign of Eq. (2.10) using a relatively large interpolation step and, from this estimation, we restart the search with a smaller interpolation step. We terminate this iterative search once the error bars do not further decrease upon reducing the interpolation step size. The estimates for zeros at T_c and below T_c are listed in Tables II, III, and IV, respectively.

The scaling dependency of the zeros on the system size is obtained by fitting to

$$r_j(L) = a + bL^{-c}(1 + fL^{-e}). \tag{4.1}$$

In the absence of the Yang-Lee edge (i.e., at criticality and in the ferromagnetic phase), we expect that a should be compatible with zero. At the critical point, Eq. (2.24) predicts that $c = \Delta/\nu$ and $e = \omega$. In the ferromagnetic regime, on the other hand, we expect $c = 3$ and $e = 1$. In the paramagnetic region, where the Yang-Lee edge is manifest, accurate estimates for the zeros should generate a nonvanishing value for a.

The FSS for the first four zeros at $T = T_c$ using the full magnetization ($|\boldsymbol{M}|$), through solving Eq. (2.10), is given in Fig. 3. A fit to the form (4.1) clearly points to a value $a \approx 0$. Fixing this value for a and also fixing $e = \omega = 0.79$ leads to the estimates for Δ/ν listed in Table V. All of the estimates are in agreement with the estimate $\Delta/\nu = 2.481\,1(2)$ coming from Ref. [6]. Fixing $f = 0$, on the other hand, leads to unacceptable fits. In this table we also present results whereby the zeros are obtained using just one of the individual components of the magnetization vector, in this case M_x. Clearly the scaling results do not depend on the selection of a specific component.

Next, we have tried a global fit to Eq. (4.1), i.e., we have enforced that the exponents c and e are the same for the first four zeros (for a detailed description of the procedure of the global fit, see, for instance, [25]). We have obtained a good fit ($\chi^2/\text{ndf} = 22.3/14$, using only the lattice sizes with $L \geqslant 12$) with $c = \Delta/\nu = 2.479\,4(9)$ and $e = \omega = 0.80(25)$. In addition, we have repeated the previous procedure but fixing c to $\Delta/\nu = 2.481\,1(2)$ (the most accurate value reported in the literature), obtaining an acceptable fit ($\chi^2/\text{ndf} = 23/15$, using only the lattice sizes with $L \geqslant 12$), which provides $\omega = 1.24(8)[10]$ (the second error bar in ω are induced by the error bar in Δ/ν). The values of Δ/ν and ω are in very good agreement with the published values.[3]

Next we study the FSS of the zeros below the critical temperature. The FSS behavior is plotted in Fig. 4. Again, we obtain clear indications that $a = 0$, as expected, and again, we do not obtain acceptable fits for the remaining scaling if we do not include a correction-to-scaling term. Fitting for both the leading and subleading behavior delivers the estimates listed Table VI. The leading scaling exponent is clearly equal to 3 in each case, and the correction exponents are very close to 1, indicating the presence of Goldstone modes, as discussed around Eq. (2.23). We have also tried in the ferromagnetic phase a global fit of the four first zeros (as described above) for the $T = 2T_c/3$ case, obtaining $c = 3.000\,20(4)$ and $e = 0.967\,5(25)$ (with $\chi^2/\text{ndf} = 0.586\,4/2$, using $L \geqslant 12$). The very residual discrepancies are due to the presence of the longitudinal mode (which would induce $1/L^2$ corrections).

[3]In numerical simulations of the Heisenberg model was obtained: $\omega = 0.64(13)$ and $\omega = 0.71(15)$ [26] and $\omega = 0.96(15)$ and $1.07(9)$ [5]. Simulating a model in the same Universality class was obtained: $\omega = 0.782(13)$ and $0.794(18)$ [27].

TABLE III. The first four LY zeros for different lattice sizes at $T = T_c/2$.

L	$r_1(L)$	$r_2(L)$	$r_3(L)$	$r_4(L)$
8	0.00378744(2)	0.01136228(5)	0.01893702(8)	0.0265116(1)
12	0.001133597(3)	0.003400788(9)	0.00566797(2)	0.00793514(2)
16	0.0004806650(8)	0.001441994(2)	0.002403321(4)	0.003364646(6)
24	0.0001431430(2)	0.0004294297(6)	0.000715716(1)	0.001002002(1)
32	0.00006054220(4)	0.0001816267(1)	0.0003027111(2)	0.0004237954(3)
48	0.000017984100(9)	0.00005395236(3)	0.00008992060(5)	0.00012588883(7)
64	0.000007596710(4)	0.00002279013(1)	0.00003798356(2)	0.00005317698(2)

TABLE IV. The first four LY zeros for different lattice sizes at $T = 2T_c/3$.

L	$r_1(L)$	$r_2(L)$	$r_3(L)$	$r_4(L)$
8	0.00424297(3)	0.01272866(8)	0.0212137(1)	0.02969766(18)
12	0.001278891(5)	0.00383666(2)	0.00639437(2)	0.008952016(34)
16	0.000544175(2)	0.001632521(7)	0.00272086(1)	0.003809186(16)
24	0.0001626250(4)	0.000487875(1)	0.000813124(2)	0.001138372(3)
32	0.0000689022(1)	0.0002067065(3)	0.0003445107(5)	0.0004823147(7)
48	0.00002050330(2)	0.00006150994(6)	0.0001025166(1)	0.0001435232(2)
64	0.000008668430(7)	0.00002600530(2))	0.00004334215(4)	0.00006067901(5)

We also investigate scaling with the index of the zeros, beginning with the ferromagnetic region. There, Eq. (2.24) predicts

$$\frac{r_j(L)}{r_1(L)} = \frac{j-\epsilon}{1-\epsilon}. \tag{4.2}$$

This is also investigated in Fig. 5 for two values of $T < T_c$. The two panels clearly indicate that r_j/r_1 is independent of T and of L. Moreover, their numerical values indicate that

$$\epsilon = \tfrac{1}{2} \quad \text{for} \quad T < T_c. \tag{4.3}$$

Therefore the functional form involving the fractional number of zeros, previously suggested at criticality, extends to the ferromagnetic region too.

The j dependency at the critical point is investigated in Fig. 6. One observes that $r_j(L)/r_1(L)$ is also independent of L at T_c. The values of $r_j(L)/r_1(L)$ are, however, less easy to interpret than they were in the ferromagnetic case. The counterpart to Eq. (4.2) is

$$\frac{r_j(L)}{r_1(L)} = \left(\frac{j-\epsilon}{1-\epsilon}\right)^{\frac{\Delta}{\nu d}} \left\{1 + \mathcal{O}\left(\frac{j-\epsilon}{L^d}\right)^{\frac{\omega}{d}}\right\}, \tag{4.4}$$

and attempts to extract a precise estimate for ϵ from this formula are beset by large errors. Indeed, we cannot discount a functional dependency of ϵ on j. Instead the full dependency may be interpreted in terms of the density of zeros, and this is analyzed in Sec. V.

Numerical determination of the locations of the LY zeros in the paramagnetic phase is hampered by considerable limitations in algorithmic accuracy. In fact, these problems are intrinsically so severe as to yield spurious zeros and hinder meaningful analysis of the Yang-Lee edge. For this reason, we relegate the discussion to the Appendix.

V. DENSITY OF ZEROS

A numerical approach to the determination of the density of partition function zeros was developed in Refs. [24,28]. The cumulative density for a finite-size system is defined as

$$G[r_j(T;L)] = \frac{2j-1}{2L^d}. \tag{5.1}$$

At the infinite-volume critical point T_c this scales in the LY case as

$$G(r) \sim r^{\frac{1}{\delta}+1} = r^{\frac{\nu d}{\Delta}}, \tag{5.2}$$

which is compatible with the compact description of scaling given in Sec. II B. In the ferromagnetic regime, on the other hand, one expects the linear behavior [24,28],

$$G(r) \sim r. \tag{5.3}$$

Differentiating Eq. (5.2) gives a density of zeros $g(r) \sim r^{1/\delta}$, commensurate with the magnetic scaling form $m_\infty(T_c,h) \sim h^{\frac{1}{\delta}}$. Differentiating Eq. (5.3), on the other hand, gives a non-vanishing density of zeros, ensuring a discontinuous transition across $h = 0$. Here, we wish to test these expectations for the three-dimensional Heisenberg model. To do this, we fit our numerical data to the form

$$G_L[r_j(L)] = a_1[r_j(L)]^{a_2} + a_3, \tag{5.4}$$

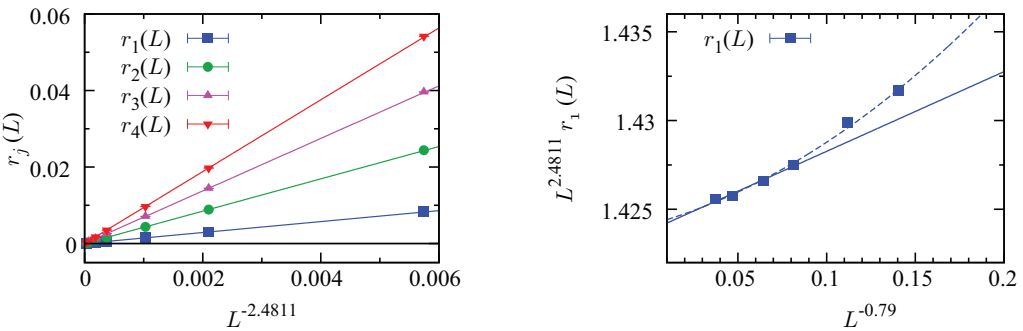

FIG. 3. (Color online) Scaling of the first four LY zeros at the critical temperature. The left panel confirms the leading finite-size scaling at the critical point as $\chi_L(0) \sim L^{\Delta/\nu} = L^{-2.4811}$ following Eq. (2.20). The right panel lends support for the accepted value of the finite-size correction exponent $\omega = 0.79$. There the dashed line includes next-to-leading scaling corrections in the fit. The error bars are smaller than the size of the symbols.

TABLE V. Scaling exponent of the LY zeros measured at the critical temperature. The estimates for the critical exponents are independent of the manner in which the zeros were determined, indicated by Eq. (2.10) and Eq. (2.11). ndf is the number of degrees of freedom of the fit.

	$T = T_c$			
	$\langle\cos(r\lvert\boldsymbol{M}\rvert)\rangle = 0$		$\langle\cos(rM_x)\rangle = 0$	
	$c = \Delta/\nu$	χ^2/ndf	$c = \Delta/\nu$	χ^2/ndf
$r_1(L)$	2.4774(12)	0.11/2	2.4792(7)	2.57/5
$r_2(L)$	2.4789(28)	2.52/4	2.4845(17)	0.52/4
$r_3(L)$	2.4791(3)	5.36/4	2.4811(26)	0.89/5
$r_4(L)$	2.4793(4)	5.48/4	2.4779(52)	4.98/5

where the coefficients depend on the temperature. We employ the fitting procedure used in Refs. [24] and [28], whereby in the absence of error bars for the density estimates in Eq. (5.1), one assumes an error of σ/L^d and then tunes σ to deliver a best fit with χ-squared per degree of freedom of one. This method delivers error estimates for the fitted parameters but precludes an independent goodness-of-fit test.

The data are plotted Fig. 7 for $T = T_c/2$, $T = 2T_c/3$, and $T = T_c$. Fitting to Eq. (5.4) yields $a_3 \approx 10^{-7} \pm 10^{-7}$ in each case. For the ferromagnetic data, fixing $a_3 = 0$ and fitting for the remaining parameters delivers a_2 compatible with 1 and supportive of Eq. (5.3). ($a_2 = 1.004(1)$ and $a_2 = 1.007(1)$ for $T = T_c/2$ and $T = 2T_c/3$, respectively, when all data points are included in the fits, reducing to $a_2 = 1.001(1)$ and $a_2 = 1.002(1)$ when only the eight points closest to the origin are used in the fits.) At the critical point itself, using all data, one estimates $a_2 = 1.203(5)$. In comparison, the estimate $\eta = 0.037\,8(9)$ from Ref. [6] delivers $a_2 = \nu d/\Delta = 2d/(d+2-\eta) = 1.209\,1(1)$.

TABLE VI. Scaling and correction to scaling exponents, c and e in Eq. (4.1), obtained from the LY zeros below the critical temperature. The results confirm the prediction $c = d = 3$ and $e = 1$ from Eq. (2.24).

	$T = T_c/2$			$T = 2T_c/3$		
	c	e	χ^2/ndf	c	e	χ^2/ndf
$r_1(L)$	3.00024(8)	0.962(7)	2.98/2	3.0006(2)	0.949(8)	3.88/2
$r_2(L)$	3.00023(8)	0.963(7)	2.06/2	3.0005(2)	0.952(9)	3.68/2
$r_3(L)$	3.00022(8)	0.964(7)	1.78/2	3.0004(2)	0.956(9)	2.92/2
$r_4(L)$	3.00021(8)	0.965(7)	1.51/2	3.0003(2)	0.962(9)	1.84/2

While the density plots give a reasonable collapse in lattice sizes, we can also analyze each L independently for greater precision. In Table VII we report the exponents we have obtained assuming a fit, including scaling corrections, of the form

$$r_j(L) = b_1 G_L^{b_2}\left(1 + b_3 G_L^{b_4}\right), \tag{5.5}$$

using error bars in $r_j(L)$ and not in G_L. With $a_2 = 1/b_2$ and $\omega = db_4$, we have also obtained reasonable agreement with the value $\omega \simeq 0.8$ quoted in the literature [7].

Finally, although there is no order parameter for the finite-size system, according to Lee and Yang's fundamental theory of phase transitions, one can relate the density of zeros to the value of the spontaneous magnetization and one expects [8]

$$M_{\rm sp} = \pi a_1. \tag{5.6}$$

We compare measurements of $M_{\rm sp}$ via Eq. (5.6) with direct estimates of $M_{\rm sp} = \langle|\boldsymbol{M}|\rangle$, where $\boldsymbol{M}$ is defined in Eq. (2.3).

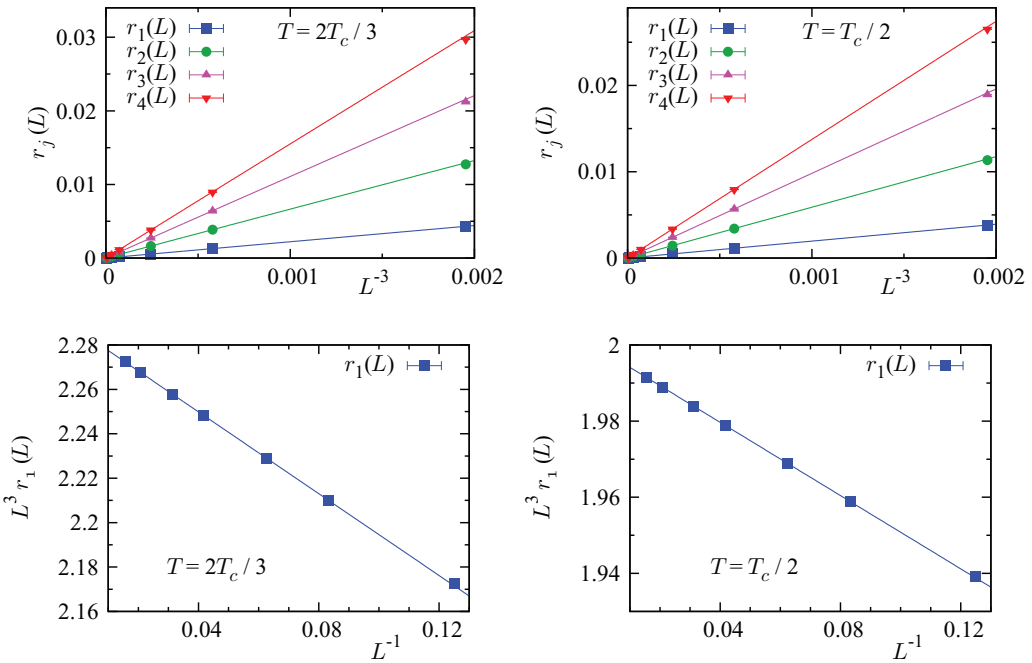

FIG. 4. (Color online) Scaling of the first four LY zeros below the critical temperature. The upper panels confirm the leading finite-size scaling at the critical point as $\chi_L(0) \sim L^{-d} = L^{-3}$. The bottom panels confirm that the associated correction term is L^{-1}, indicative of the presence of Goldstone bosons. The error bars are smaller than the size of the symbols.

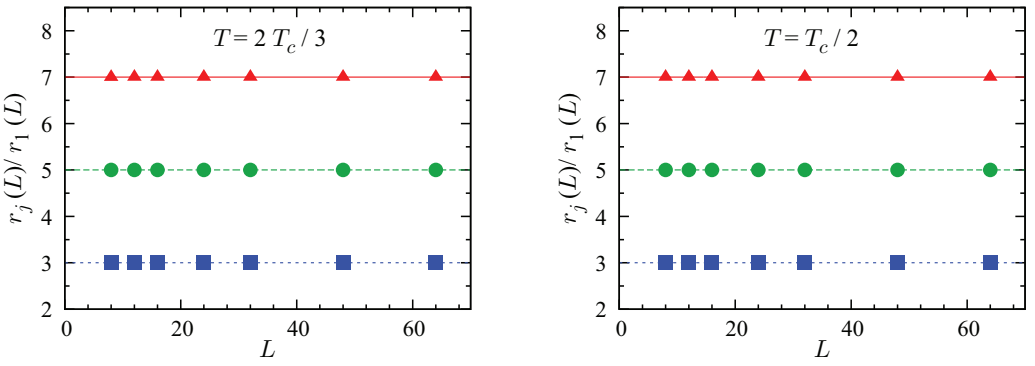

FIG. 5. (Color online) The ratios r_4/r_1 (triangles), r_3/r_1 (circles), and r_2/r_1 (squares) below the critical temperature. The error bars are smaller than the symbol size. The ratios $r_j(L)/r_1(L)$ are independent of L in the ferromagnetic phase and are, in fact, $2j-1$.

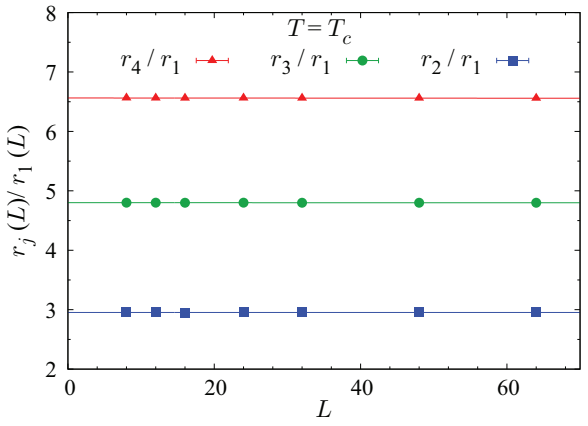

FIG. 6. (Color online) At the critical point the ratio $r_j(L)/r_1(L)$ is also independent of L. The error bars are smaller than the symbol size in every case.

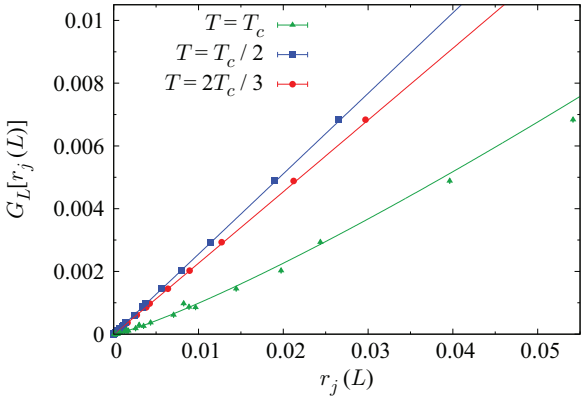

FIG. 7. (Color online) The density of zeros for at $T = T_c/2$ (blue squares), $T = 2T_c/3$ (red circles), and at $T = T_c$ (green triangles). The error bars are smaller than the symbol size.

We perform the comparison using the full data sets for each $T < T_c$, as well as for each lattice size independently. We have checked that the data for each lattice follows a straight line according with the theoretical expectation and present our results in Table VIII. We list in Table VIII the different estimates of the spontaneous magnetization for $T < T_c$ for the different lattice sizes. The agreement between them is excellent.

VI. CONCLUSIONS

We have performed a numerical analysis of the Heisenberg model in three dimensions, paying special attention to the LY zeros, the scaling properties of which contain information on Goldstone modes. Besides FSS for individual zeros in the critical and paramagnetic regimes, we have looked at the index of zeros and shown that a comprehensive description extends to both regions. This allows us to obtain very precise estimates for the critical exponents and correction-to-scaling terms.

A first attempt to numerically examine scaling associated with the Yang-Lee edge in the paramagnetic region encounters obstacles which we elucidate directly and through analogy with the one-dimensional Ising model.

We confirm that study of the density of zeros for finite size offers a compact and very accurate way to investigate the onset of spontaneous magnetization, although the latter is only manifest in infinite volume. Moreover, we have obtained a good estimate of the correction-to-scaling exponent using the behavior of the density of zeros. Finally, we have found that the discretization method proposed for the density of zeros (which induces the factor $2j-1$) in the literature works really well

TABLE VII. a_2 and ω from the density of zeros via Eq. (5.5).

j	a_2	ω
1	1.2097(4)	0.9(3)
2	1.2094(3)	1.1(2)
3	1.2092(2)	1.23(6)
4	1.2090(3)	1.3(3)

TABLE VIII. Sample averaged spontaneous magnetization below the critical temperature measured directly and measured via Eq. (5.6) below the critical temperature using data for each lattice size individually.

	M_{sp} measured directly		M_{sp} measured via density	
L	$T = 2T_c/3$	$T = T_c/2$	$T = 2T_c/3$	$T = T_c/2$
8	0.723070(4)	0.810036(3)	0.723078(3)	0.810038(3)
12	0.710792(3)	0.801895(2)	0.710794(2)	0.801898(2)
16	0.704728(3)	0.797844(1)	0.7047315(20)	0.7978451(7)
24	0.698713(2)	0.793808(1)	0.6987122(8)	0.7938082(6)
32	0.695724(1)	0.791793(1)	0.6957245(5)	0.7917944(3)
64	0.691257(1)	0.7887771(4)	0.6912572(3)	0.7887785(2)

only in the ferromagnetic phase but is at best an approximation at the critical point.

ACKNOWLEDGMENTS

This research was supported by a Marie Curie International Incoming Fellowship and International Research Staff Exchange Scheme grants within the 7th European Community Framework Program. A.G.G. and J.J.R. acknowledge support from Research Contracts No. FIS2010-16587 (MICINN), No. GR101583 (Junta de Extremadura), and No. PIRSES-GA-2011-295302 (European Union). R.K. thanks Nickolay Izmailian for discussions.

APPENDIX: SPURIOUS ZEROS IN THE PARAMAGNETIC PHASE

Figure 8 shows the evolution of the expectation of the cosine in Eq. (2.11) through which the zeros are detected. One notices

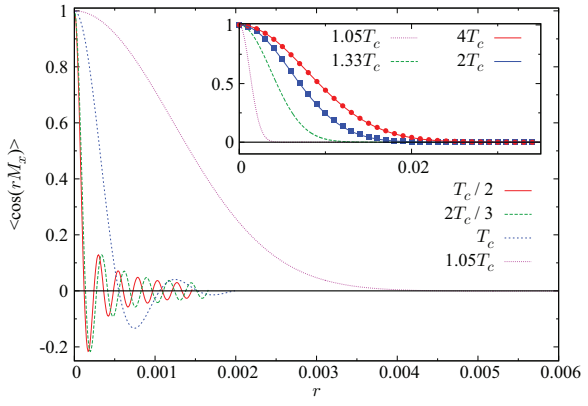

FIG. 8. (Color online) Behavior of $\langle \cos(rM_x)\rangle$ for the three-dimensional Heisenberg model with $L = 32$ below, at, and above criticality. In the inset, we have also plotted the same quantity in the paramagnetic phase in order to show the very different behavior there. For the sake of clarity, we only plot the lines joining the data points, except for the two highest temperatures (in the inset) in which real data points are plotted. For these highest temperatures we also plotted the prediction from the Gaussian approximation (red and blue continuous lines) [see Eq. (A3)]. There are no free parameters, since we have used the susceptibility which was computed numerically. Notice the good agreement.

a remarkable difference between the amplitudes of the function below and above criticality; in the paramagnetic phase the amplitude of $\langle \cos(rM_x)\rangle$ is dampened as r increases, an effect not present at or below criticality. This leads to algorithmic detection of spurious LY zeros in the symmetric phase.

That the detected zeros are indeed spurious is indicated first by a straightforward fit to Eq. (4.1), which delivers $a \approx 0$. The fact that the estimated zeros do not settle onto a Yang-Lee edge already hints that they are spurious. A second feature is that the scaling appears to indicate a leading exponent $c \approx 1.5 = d/2$. That this is also spurious is indicated as follows.

It is well known that the probability distribution of the magnetization in the paramagnetic phase follows an approximate Gaussian probability distribution. We write this distribution as (considering a single dimension here for simplicity)

$$P(M) = \frac{1}{\sqrt{2\pi V \chi_L^{(\mathrm{nc})}}} \exp\left[-\frac{M^2}{2\chi_L^{(\mathrm{nc})} V}\right], \tag{A1}$$

where M is the total magnetization, V is the volume, and $\chi_L^{(\mathrm{nc})} = \langle M^2\rangle / V$ is the susceptibility, which is finite in the paramagnetic phase. The algorithm detects zeros through Eq. (2.11), and with the Gaussian distribution governing the high-temperature phase,

$$\langle \cos(rM)\rangle = \exp\left[-\frac{1}{2}\chi_L^{(\mathrm{nc})} V r^2\right] \tag{A2}$$

there. Here we have assumed $V \gg 1$ (otherwise this result would be modulated by an error-function factor). Therefore $\langle \cos(rM)\rangle$ decays exponentially quickly in the paramagnetic phase.[4] The reader can see the suitability of the Gaussian approximation in the inset of Fig. 8.

Numerically we compute $c(r) = \langle \cos(rM)\rangle$ with a given statistical error (which is also r dependent) that we will denote $\delta(r)$. When $c(r_*) \sim \delta(r_*)$, a statistical fluctuation can induce a spurious zero at r_*. Hence, if we have similar error bars for all the lattice sizes, this implies [see Eq. (A2)] that the spurious zero scales as $1/\sqrt{V}$. This explains the origin and scaling of the spurious paramagnetic zeros—the behavior is simply due to finite statistics associated with the numerical approach. Instead, if we improve the statistics, reducing the value of $\delta(r_*)$, the spurious zero should disappear.

We can gain further insight by examining slope of $\langle \cos(rM)\rangle$, which is

$$\frac{d}{dr}\langle \cos(rM)\rangle = -\langle M \sin(rM)\rangle. \tag{A4}$$

We can examine this slope in the three different regimes. At and below the critical point, we use the fact that $M \simeq \sqrt{\langle M^2\rangle}$ to see that in both cases $r_1 M$ is $O(1)$, where r_1 is a genuine zero (and having used the scaling of the zeros in each of these two regions). Therefore, close to r_1,

$$\left.\frac{d}{dr}\langle \cos(rM)\rangle\right|_{r_1} \sim |M|. \tag{A5}$$

[4] In O(N) models, one obtains

$$\langle \cos(rM_x)\rangle = \exp\left[-\frac{1}{2N}\chi_L^{(\mathrm{nc})} V r^2\right]. \tag{A3}$$

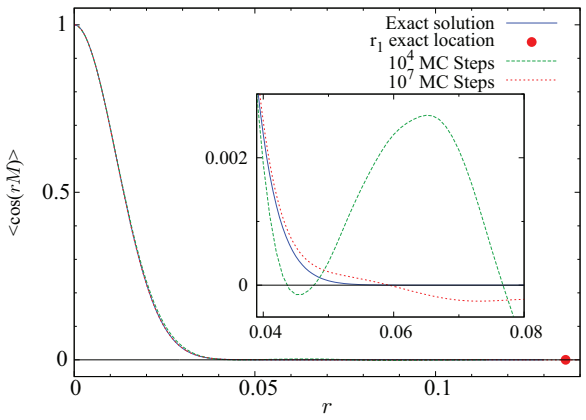

FIG. 9. (Color online) Behavior of $\langle \cos(rM) \rangle$ for the one-dimensional Ising model with $L = 1000$ above criticality, i.e., above $T = 0$. The exact zero is indicated by the red disk and the exact solution by a blue line. The numerical algorithm, however, detects spurious zeros, as can be seen in the inset.

Since $|M| \sim V$ in the ferromagnetic phase, and its typical value at criticality is $|M| \simeq \sqrt{\langle M^2 \rangle} = \sqrt{V \chi_L^{(\mathrm{nc})}}$, it is clear that at and below the critical temperature the slope is large. Since the algorithm detects zeros through changes in the sign of $\langle \cos(rM) \rangle$, it is robust in the critical and ferromagnetic regions. In the paramagnetic region, however, the Gaussian approximation gives

$$\left. \frac{d}{dr} \langle \cos(rM) \rangle \right|_{r_1} = -r_1 V \chi \exp\left[-\frac{1}{2} \chi V r_1^2 \right]. \quad \text{(A6)}$$

This gives an exponentially depressed slope in the paramagnetic phase, rendering detection of genuine zeros difficult and spurious zeros (as noise) feasible.

To check the above interpretation, we refer to the Ising model in one dimension, where the partition function in a magnetic field can be analytically determined using periodic boundary conditions and where the entire $T > 0$ region is paramagnetic [8]. The two eigenvalues of the transfer matrix are

$$\lambda_\pm(\beta, H) = e^\beta [\cosh(H) \pm \sqrt{e^{-4\beta} + \sinh^2(H)}], \quad \text{(A7)}$$

and the partition function of a chain of L spins is

$$Z(\beta, H) = \lambda_+(\beta, H)^L + \lambda_-(\beta, H)^L. \quad \text{(A8)}$$

By introducing a pure imaginary magnetic field by defining $H = ir$, the eigenvalues can be written

$$\lambda_\pm(\beta, ir) = e^\beta [\cos(r) \pm \sqrt{e^{-4\beta} - \sin^2(r)}]. \quad \text{(A9)}$$

Notice that for $e^{-2\beta} < \sin^2(r)$, the eigenvalues $\lambda_\pm$ are complex numbers but satisfying $\lambda_+^* = \lambda_-$. This confirms our earlier statement that the partition function in a pure imaginary magnetic field is real. One finds [29]

$$\langle \cos(rM) \rangle = \frac{Z(\beta, ir)}{Z(\beta, 0)} = \frac{\lambda_+(\beta, ir)^L + \lambda_-(\beta, ir)^L}{\lambda_+(\beta, 0)^L + \lambda_-(\beta, 0)^L}. \quad \text{(A10)}$$

Therefore the zeros in the paramagnetic phase of the one-dimensional Ising model can be exactly determined. In Fig. 9, the first zero for such a system is depicted as a disk (red online). This figure also depicts the results for $\langle \cos(rM) \rangle$ from two Monte Carlo simulations and for the exact solution. As expected, the numerically computed $\langle \cos(rM) \rangle$ decays rapidly with increasing r; it then remains very close to zero and traverses the axis well before the true zero is reached (green line). Although the situation improves with increased numerical accuracy (see red line), the figure clearly demonstrates that the Yang-Lee edge is not reliably accessible using this numerical technique.

[1] M. N. Barber, in *Phase Transitions and Critical Phenomena*, edited by C. Domb and J. L. Lebowitz (Academic, New York, 1983), Vol. 8.

[2] M. H. Phan, V. Francoa, N. S. Bingham, H. Srikanth, N. H. Hur, and S. C. Yu, J. Alloys Compd. **508**, 238 (2010).

[3] N. Dhahri, J. Dhahri, E. K. Hlil, and E. Dhahri, J. Magn. Magn. Mater. **324**, 806 (2012).

[4] M. Campostrini, M. Hasenbusch, A. Pelissetto, P. Rossi, and E. Vicari, Phys. Rev. B **65**, 144520 (2002).

[5] A. Gordillo-Guerrero and J. J. Ruiz-Lorenzo, J. Stat. Mech.: Theory Exp. (2007) P06014.

[6] M. Hasenbusch and E. Vicari, Phys. Rev. B **84**, 125136 (2011).

[7] A. Pelissetto and E. Vicari, Phys. Rep. **368**, 549 (2002).

[8] C. N. Yang and T. D. Lee, Phys. Rev. **87**, 404 (1952); T. D. Lee and C. N. Yang, *ibid.* **87**, 410 (1952).

[9] D. Amit and V. Martín-Mayor, *Field Theory, the Renormalization Group, and Critical Phenomena: Graphs to Computers* (World Scientific, Singapore, 2005).

[10] M. E. Fisher and V. Privman, Phys. Rev. B **32**, 447 (1985).

[11] P. Hasenfratz and H. Leutwyler, Nucl. Phys. B **343**, 241 (1990).

[12] I. Dimitrovic, P. Hasenfratz, J. Nager, and F. Niedermayer, Nucl. Phys. B **350**, 893 (1991).

[13] V. Dohm, Phys. Rev. Lett. **110**, 107207 (2013).

[14] Ch. Binek, Phys. Rev. Lett. **81**, 5644 (1998); B. B. Wei and R.-B. Liu, *ibid.* **109**, 185701 (2012).

[15] A. J. Bray, Phys. Rev. Lett. **59**, 586 (1987).

[16] R. B. Griffiths, Phys. Rev. Lett. **23**, 17 (1969).

[17] M. B. Salamon, P. Lin, and S. H. Chun, Phys. Rev. Lett. **88**, 197203 (2002).

[18] F. Y. Wu, Int. J. Modern Phys. B **22**, 1899 (2008).

[19] G. Gallavotti, S. Miracle–Sole, and D. W. Robinson, Phys. Lett. A **25**, 493 (1967); Commun. Math. Phys. **10**, 311 (1968).

[20] M. E. Fisher, Phys. Rev. Lett. **40**, 1610 (1978).

[21] T. Asano, Phys. Rev. Lett. **24**, 1409 (1970).

[22] J. J. Ruiz-Lorenzo, J. Phys. A **30**, 485 (1997).

[23] C. Itzykson, R. B. Pearson, and J. B. Zuber, Nucl. Phys. B **220**, 415 (1983).

[24] W. Janke and R. Kenna, J. Stat. Phys. **102**, 1211 (2001).

[25] R. A. Baños, J. M. Gil-Narvion, J. Monforte-Garcia, J. J. Ruiz-Lorenzo, and D. Yllanes, J. Stat. Mech.: Theory Exp. (2013) P02031.
[26] H. G. Ballesteros, L. A. Fernández, V. Martín-Mayor, and A. Muñoz-Sudupe, Phys. Lett. B **387**, 125 (1996).
[27] M. Hasenbusch, J. Phys. A **34**, 8221 (2001).
[28] W. Janke, D. A. Johnston, and R. Kenna, Nucl. Phys. B **682**, 618 (2004).
[29] D. A. Kurtze and M. E. Fisher, J. Stat. Phys. **19**, 205 (1978); Phys. Rev. B **20**, 2785 (1979).